Differential theory of diffraction by finite cylindrical objects

Nicolas Bonod, Evgeny Popov, and Michel Nevière

Institut Fresnel, Unité Mixte de Recherche Associée au Centre National de la Recherche Scientifique No. 6133, Université de Provence, Faculté des Sciences et Techniques de St. Jérôme, Avenue Escadrille Normandie Niémen, 13397 Marseille Cedex 20, France

Received June 16, 2004; revised manuscript received September 16, 2004; accepted October 1, 2004

We present a differential theory for solving Maxwell equations in cylindrical coordinates, projecting them onto a Fourier–Bessel basis. Numerical calculations require the truncation of that basis, so that correct rules of factorization have to be used. The convergence of the method is studied for different cases of dielectric and metallic cylinders of finite length. Applications of such a method are presented, with a special emphasis on the near-field map inside a hole pierced in a plane metallic film. © 2005 Optical Society of America

OCIS codes: 050.1960, 050.1220, 260.1960, 260.2110.

1. INTRODUCTION

The differential method has been used with great success in diffraction grating theory.[1,2] In the case of infinite gratings, Maxwell equations are projected onto a discrete Fourier basis,[2,3] while for finite gratings or aperiodic objects, Maxwell equations are projected onto a continuous Fourier basis.[4] The differential method has already been developed in cylindrical coordinates to analyze the diffraction of a plane wave by infinitely long rods.[2] Maxwell equations are in that case also projected onto a discrete Fourier basis. However, in many cases, the diffraction system consists of cylindrical objects having finite length, for example, light transmission through a single subwavelength hole in a metallic screen. We show in this paper how to solve Maxwell equations when the diffracting structure is invariant with respect to the polar angle θ, modulated (not necessarily periodically) with respect to the variable r, and has a finite thickness along the z coordinate. First, the electromagnetic field is projected onto a cylindrical spatial coordinate basis. Then the periodicity along the variable θ allows us to develop the electromagnetic field into Fourier series.[2] Maxwell equations then lead to Helmholtz equations for the Fourier components, with solutions represented as linear sums of Bessel functions. This basis is called Fourier–Bessel basis.[5] The numerical treatment of the method requires dealing only with finite and discrete basis of functions. As is now well known, the manner of factorizing products of functions onto such a basis depends on the continuity of the functions and of their products.[6,7] We show how to apply correct rules of factorization of products appearing in Maxwell equations in the specific case of a Bessel-function basis. The method can analyze various types of diffracting devices, such as Fresnel lenses or a single hole.

2. HELMHOLTZ EQUATIONS IN CYLINDRICAL COORDINATES PROJECTED ONTO A FOURIER BASIS

Let us write the harmonic Maxwell equations, assuming an $\exp(-i\omega t)$ time dependence:

$$\operatorname{curl} \mathbf{E}(\mathbf{r}) = i\omega\mu_0 \mathbf{H}(\mathbf{r}), \tag{1}$$

$$\operatorname{curl} \mathbf{H}(\mathbf{r}) = -i\omega\epsilon(\mathbf{r})\mathbf{E}(\mathbf{r}). \tag{2}$$

In cylindrical coordinates (r, θ, z), any device and field component is periodic with respect to the polar angle θ, with period 2π. We study structures that have cylindrical symmetry and are piecewise invariant along z. Representing the electromagnetic field by Fourier series, Eqs. (1) and (2) become

$$\operatorname{curl} \sum_{n=-\infty}^{\infty} \mathbf{E}_n(r, z)\exp(in\theta) = i\omega\mu_0 \sum_{n=-\infty}^{\infty} \mathbf{H}_n(r, z) \times \exp(in\theta), \tag{3}$$

$$\operatorname{curl} \sum_{n=-\infty}^{\infty} \mathbf{H}_n(r, z)\exp(in\theta) = -i\omega\epsilon(r, z) \sum_{n=-\infty}^{\infty} \mathbf{E}_n(r, z) \times \exp(in\theta). \tag{4}$$

The independence of ϵ with respect to the variable θ and the orthogonality of the Fourier basis lead to separation of equations for each value of n:

$$\sum_{n=-\infty}^{\infty} [\mathrm{curl}\,\mathbf{E}_n(r, z) + in\hat{\boldsymbol{\theta}} \wedge \mathbf{E}_n(r, z)]\exp(in\theta) = \sum_{n=-\infty}^{\infty} i\omega\mu_0 \mathbf{H}_n(r, z)\exp(in\theta), \quad (5)$$

$$\sum_{n=-\infty}^{\infty} [\mathrm{curl}\,\mathbf{H}_n(r, z) + in\hat{\boldsymbol{\theta}} \wedge \mathbf{H}_n(r, z)]\exp(in\theta) = -\sum_{n=-\infty}^{\infty} i\omega\epsilon(r, z)\mathbf{E}_n(r, z)\exp(in\theta). \quad (6)$$

The components of the electric-field vector on the cylindrical coordinates (r, θ, z) are written as E_r, E_θ, E_z, and their Fourier components verify the following coupled equations:

$$\Delta E_{r,n} - \frac{E_{r,n}}{r^2} + \omega^2\mu_0\epsilon(r)E_{r,n} - \frac{2in}{r^2}E_{\theta,n} = 0, \quad (7)$$

$$\Delta E_{\theta,n} - \frac{E_{\theta,n}}{r^2} + \omega^2\mu_0\epsilon(r)E_{\theta,n} + \frac{2in}{r^2}E_{r,n} = 0. \quad (8)$$

Using the notation

$$E_{\theta,n} + iE_{r,n} = E_n^+, \quad (9)$$

$$E_{\theta,n} - iE_{r,n} = E_n^-, \quad (10)$$

Eqs. (7) and (8) immediately give

$$\Delta E_n^+ - \frac{E_n^+}{r^2} + \omega^2\mu_0\epsilon(r)E_n^+ + \frac{2n}{r^2}E_n^+ = 0, \quad (11)$$

$$\Delta E_n^- - \frac{E_n^-}{r^2} + \omega^2\mu_0\epsilon(r)E_n^- - \frac{2n}{r^2}E_n^- = 0. \quad (12)$$

The general solutions of these differential equations can be written in terms of Bessel-function expansion:

$$E_n^+ = E_{\theta,n} + iE_{r,n} = \int_{k_r=0}^{\infty} 2c_n^E(k_r, z)J_{n-1}(k_r r)k_r \mathrm{d}k_r, \quad (13)$$

$$E_n^- = E_{\theta,n} - iE_{r,n} = \int_{k_r=0}^{\infty} 2b_n^E(k_r, z)J_{n+1}(k_r r)k_r \mathrm{d}k_r, \quad (14)$$

k_r being the radial wave number. The numerical calculations require truncating the basis of projection. This means that we have to replace the integrals in Eqs. (13) and (14) by discrete sums bounded by a finite limit. In addition, the infinite limits of summations in Eqs. (5) and (6) become finite. The following substitutions are made:

$$\int_{k_r=0}^{\infty} k_r \mathrm{d}k_r \to \sum_{m=1}^{\mathrm{Max}} k_m \Delta k_m, \quad (15)$$

$$\sum_{n=-\infty}^{+\infty} \to \sum_{n=-N}^{+N}. \quad (16)$$

The discretization step Δk_m is equal to $k_{m+1} - k_m$ and can depend on m. In Section 5, it will be taken as a constant and written as Δk_r. Moreover, the unknown functions $b_n^E(k_r, z)$ and $c_n^E(k_r, z)$ are turned into sets of discrete unknowns denoted by $b_{n,m}^E(z)$ and $c_{n,m}^E(z)$. Summing or subtracting Eqs. (13) and (14), we obtain

$$E_r(r, z) = i\sum_{n=-N}^{N}\sum_{m=1}^{\mathrm{Max}} k_m\Delta k_m[b_{n,m}^E(z)J_{n+1}(k_m r) - c_{n,m}^E(z)J_{n-1}(k_m r)]\exp(in\theta), \quad (17)$$

$$E_\theta(r, z) = \sum_{n=-N}^{N}\sum_{m=1}^{\mathrm{Max}} k_m\Delta k_m[b_{n,m}^E(z)J_{n+1}(k_m r) + c_{n,m}^E(z)J_{n-1}(k_m r)]\exp(in\theta). \quad (18)$$

Similar calculations for the magnetic field components lead to

$$H_r(r, z) = i\sum_{n=-N}^{N}\sum_{m=1}^{\mathrm{Max}} k_m\Delta k_m[b_{n,m}^H(z)J_{n+1}(k_m r) - c_{n,m}^H(z)J_{n-1}(k_m r)]\exp(in\theta), \quad (19)$$

$$H_\theta(r, z) = \sum_{n=-N}^{N}\sum_{m=1}^{\mathrm{Max}} k_m\Delta k_m[b_{n,m}^H(z)J_{n+1}(k_m r) + c_{n,m}^H(z)J_{n-1}(k_m r)]\exp(in\theta). \quad (20)$$

The other two field components can be expressed by using Maxwell equations:

$$i\omega\mu_0 H_{z,n} = \sum_{m=1}^{\mathrm{Max}} (b_{n,m}^E - c_{n,m}^E)J_n(k_m r)k_m^2\Delta k_m, \quad (21)$$

$$-i\omega\epsilon(r)E_{z,n} = \sum_{m=1}^{\mathrm{Max}} (b_{n,m}^H - c_{n,m}^H)J_n(k_m r)k_m^2\Delta k_m. \quad (22)$$

The factorization of the product $\epsilon(r)E_{z,n}(r)$ projected onto a Bessel basis is made by using the direct rule since $E_{z,n}(r)$ is a continuous function.[7] As a consequence, we first develop $E_{z,n}(r)$ as a sum of Bessel functions:

$$E_{z,n} = \sum_{m=1}^{\mathrm{Max}} k_m\Delta k_m E_{z,n,m}J_n(k_m r). \quad (23)$$

Putting Eq. (23) into Eq. (22), multiplying the two members by $rJ_n(k_{m'}r)$ and integrating from 0 to infinity, the orthogonality of the basis leads to

$$k_{m'}[b_{n,m'}^H - c_{n,m'}^H] = -i\omega\sum_{m=1}^{\mathrm{Max}} k_m\Delta k_m E_{z,n,m} \times \int_{r=0}^{\infty} \epsilon(r)J_n(k_m r)J_n(k_{m'}r)r\mathrm{d}r. \quad (24)$$

The different scalar products of the terms $\epsilon(r)J_n(k_m r)$ (with $m \in [1, \mathrm{Max}]$) with the functions $J_n(k_{m'}r)$ (with $m' \in [1, \mathrm{Max}]$) are written in a matrix $[\epsilon]^{n,n}$, where the

first (resp. second) superscript n indicates the order of Bessel function with argument $k_m r$ (resp. $k_{m'} r$):

$$\int_{r=0}^{\infty} \epsilon(r) J_n(k_m r) J_n(k_{m'} r) r \mathrm{d}r \rightarrow [\epsilon]_{m,m'}^{n,n},$$

$$m, m' \in [1, \mathrm{Max}]. \tag{25}$$

It is more convenient to introduce the following notation:

$$[\epsilon]_{m,m'}^{n,\tilde{n}} = [\epsilon]_{m,m'}^{n,n} k_{m'} \Delta k_{m'} \quad \text{and}$$

$$[\epsilon]_{m,m'}^{\tilde{n},n} = [\epsilon]_{m,m'}^{n,n} k_m \Delta k_m \tag{26}$$

so that Eq. (24) reads as

$$k_m [b_{n,m}^H - c_{n,m}^H] = -i\omega \sum_{m'=1}^{\mathrm{Max}} E_{z,n,m'} [\epsilon]_{m,m'}^{n,\tilde{n}}. \tag{27}$$

Inverting the matrix $[\epsilon]^{n,\tilde{n}}$, we obtain the components $E_{z,n,m}$, which we substitute into Eq. (23):

$$E_{z,n} = \sum_{m=1}^{\mathrm{Max}} \frac{-k_m}{i\omega} \Delta k_m J_n(k_m r) \sum_{m'=1}^{\mathrm{Max}} ([\epsilon]_{m,m'}^{n,\tilde{n}})^{-1} k_{m'} \times [b_{n,m'}^H - c_{n,m'}^H]. \tag{28}$$

3. EXPRESSION OF AN INCIDENT PLANE WAVE IN THE FOURIER–BESSEL BASIS

We consider here two types of incident waves that are important in practice: plane waves and Gaussian beams. However, following the same lines, the method can easily be generalized to an arbitrary shaped incident wave.

A. Incident Plane Wave

Let us consider an arbitrary wave vector $\mathbf{k_i}$ with components $\mathbf{k}_{i,r}$ and $\mathbf{k}_{i,z}$ in the xOy plane and on the z axis, respectively (Fig. 1). If θ_0 is the polar angle of $\mathbf{k}_{i,r}$ in the xOy plane, then a plane incident wave is represented in a cylindrical basis in the form

$$\mathbf{E}^i = \mathbf{E}_0 \sum_{n=-\infty}^{\infty} i^n J_n(k_{i,r} r) \exp[in(\theta - \theta_0)] \exp(-ik_{i,z} z). \tag{29}$$

The expression of the amplitude vector $\mathbf{E}_0$ in the cylindrical spatial basis depends on the incident field polarization. For a linearly polarized incident wave, the Cartesian components of $\mathbf{E}_0$ are constant:

$$\mathbf{E}_0 = E_{0x}\hat{\mathbf{x}} + E_{0y}\hat{\mathbf{y}} + E_{0z}\hat{\mathbf{z}}. \tag{30}$$

Using the expression of the Cartesian unit vectors in cylindrical coordinates, we obtain

$$\mathbf{E}_0 = E_{0x}(\hat{\mathbf{r}} \cos\theta - \hat{\boldsymbol{\theta}} \sin\theta) + E_{0y}(\hat{\mathbf{r}} \sin\theta + \hat{\boldsymbol{\theta}} \cos\theta) + E_{0z}\hat{\mathbf{z}}, \tag{31}$$

or

$$\mathbf{E}_0 = \hat{\mathbf{r}}\left[\left(\frac{E_{0x}}{2} + \frac{E_{0y}}{2i}\right)\exp(i\theta) + \left(\frac{E_{0x}}{2} - \frac{E_{0y}}{2i}\right)\exp(-i\theta)\right] + \hat{\boldsymbol{\theta}}\left[\left(-\frac{E_{0x}}{2i} + \frac{E_{0y}}{2}\right)\exp(i\theta) + \left(\frac{E_{0x}}{2i} + \frac{E_{0y}}{2}\right)\exp(-i\theta)\right] + \hat{\mathbf{z}}E_{0z}. \tag{32}$$

From these expressions, one can deduce the expression of the electromagnetic components $E_r^i = \mathbf{E}^i \cdot \hat{\mathbf{r}}$ and $E_\theta^i = \mathbf{E}^i \cdot \hat{\boldsymbol{\theta}}$ of the incident plane wave:

$$E_r^i = \sum_{n=-N}^{N} \left(\frac{E_{0x}}{2} + \frac{E_{0y}}{2i}\right) i^n \exp(-in\theta_0) \times J_n(k_{i,r} r)\exp[i(n+1)\theta]\exp(-ik_{i,z} z) + \sum_{n=-N}^{N} \left(\frac{E_{0x}}{2} - \frac{E_{0y}}{2i}\right) i^n \exp(-in\theta_0) \times J_n(k_{i,r} r)\exp[i(n-1)\theta]\exp(-ik_{i,z} z). \tag{33}$$

A simple translation of the subscript n by ± 1 then leads to

$$E_r^i = \sum_{n=-N+1}^{N+1} i\left(\frac{E_{0x}}{2i} - \frac{E_{0y}}{2}\right) i^{n-1} \exp[-i(n-1)\theta_0] \times J_{n-1}(k_{i,r} r)\exp(in\theta)\exp(-ik_{i,z} z) + \sum_{n=-N-1}^{N-1} i\left(\frac{E_{0x}}{2i} + \frac{E_{0y}}{2}\right) i^{n+1} \exp(-i(n+1) \times \theta_0) J_{n+1}(k_{i,r} r)\exp(in\theta)\exp(-ik_{i,z} z), \tag{34}$$

and

$$E_\theta^i = \sum_{n=-N+1}^{N+1} \left(-\frac{E_{0x}}{2i} + \frac{E_{0y}}{2}\right) i^{n-1} \exp(-i(n-1)\theta_0) \times J_{n-1}(k_{i,r} r)\exp(in\theta)\exp(-ik_{i,z} z) + \sum_{n=-N-1}^{N-1} \left(\frac{E_{0x}}{2i} + \frac{E_{0y}}{2}\right) i^{n+1} \exp(-i(n+1)\theta_0) \times J_{n+1}(k_{i,r} r)\exp(in\theta)\exp(-ik_{i,z} z). \tag{35}$$

We write these equations with $N \gg 1$ so that $N \pm 1 \rightarrow N$, and we replace continuous variables $k_{i,r}$ and $k_{i,z}$ by discretized ones,

$$k_{i,r} = k_{m_i}, \quad k_{i,z} = k_{z,m_i}, \tag{36}$$

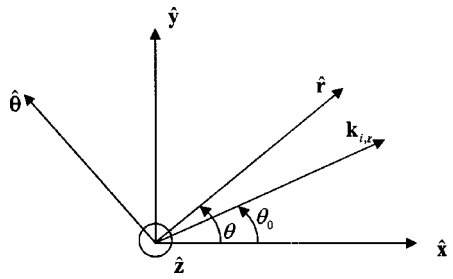

Fig. 1. Representation of the spatial cylindrical basis added to the Cartesian one. In our problem the angle θ_0 is taken equal to 0. The angle θ shows the possibility of conical incidence. The projection of the wave vector onto the Oxy plane is equal to $\mathbf{k}_{ir}$.

so that in writing Eqs. (17) and (18) with only one radial wave number k_{m_i}, we are able to identify the components of the incident electromagnetic field in a Fourier–Bessel basis:

$$\tilde{b}^E_{n,m_i} = k_{m_i} b^E_{n,m_i} = \left(\frac{E_{0x}}{2i} + \frac{E_{0y}}{2} \right) \frac{i^{n+1}}{\Delta k_{m_i}} \times \exp[-i(n+1)\theta_0] \exp(-ik_{z,m_i} z), \quad (37)$$

$$\tilde{c}^E_{n,m_i} = k_{m_i} c^E_{n,m_i} = \left(-\frac{E_{0x}}{2i} + \frac{E_{0y}}{2} \right) \frac{i^{n-1}}{\Delta k_{m_i}} \times \exp[-i(n-1)\theta_0] \exp(-ik_{z,m_i} z). \quad (38)$$

We notice the necessity of introducing the new variables $\tilde{b}^E_{n,m_i}$ and $\tilde{c}^E_{n,m_i}$ to avoid divergence of the components b^E_{n,m_i} and c^E_{n,m_i} in the case of normal incidence, where $k_{m_i} = 0$ with $m_i = 1$.

B. Incident Gaussian Beam

We first recall that a Gaussian beam is characterized by its waist w_0 and its Rayleigh diffraction length z_R with $z_R = \pi w_0^2/\lambda$, where λ is the wavelength in the superstrate. Introducing $l = 2z_R = kw_0^2$ and the dimensionless parameter $s = w_0/l$, Davis[8] showed that the usual "Gaussian formula" used to describe a Gaussian beam is an approximate solution to the homogeneous Maxwell equations valid to $o(s^2)$. Let us assume that the Gaussian beam is polarized with the electric vector in the xOz plane and has a central wave vector $\mathbf{k}_i$ parallel to the z axis (normal incidence) so that $k_{m_i} = 0$, and $k_{z,m_i} = k_i$. The electric-field components then read[8]

$$E^i_x = E_0 Q \exp(-Qh^2) \exp(-ik_{z,m_i} z), \quad (39)$$

$$E^i_z = -E_0 2i \frac{Q^2 x}{l} \exp(-Qh^2) \exp(-ik_{z,m_i} z) = -2i \frac{Qx}{l} E^i_x, \quad (40)$$

where

$$h^2 = (x^2 + y^2)/w_0^2, \quad (41)$$

$$Q = i/(2z/l + i), \quad (42)$$

and E_0 is a given field amplitude. It is worth noting that the longitudinal component E^i_z is often omitted in the textbook treatments of Gaussian beams. However, it is necessary to include it in the theory, so that the Maxwell equation $\mathrm{div}\,\mathbf{E} = 0$ can be satisfied and the boundary conditions can be fulfilled.

In the theory, we need only the expression of the incident field at $z = 0$. There, $Q = 1$, and the equations giving the Gaussian beam reduce to

$$E^i_x = E_0 \exp(-r^2/w_0^2) \exp(-ik_{z,m_i} z), \quad (43)$$

$$E^i_z = -E_0 \frac{ix}{z_R} \exp(-r^2/w_0^2) \exp(-ik_{z,m_i} z), \quad (44)$$

where $r^2 = x^2 + y^2$. Following Eq. (31), we derive

$$\mathbf{E}^i = E^i_x (\hat{\mathbf{r}} \cos\theta - \hat{\boldsymbol{\theta}} \sin\theta) + E^i_z \hat{\mathbf{z}}, \quad (45)$$

which gives

$$\mathbf{E}^i = \frac{E_0}{2} \exp(-r^2/w_0^2) \exp(-ik_{z,m_i} z) (\exp(i\theta) + \exp(-i\theta)) \hat{\mathbf{r}} - \frac{E_0}{2i} \exp(-r^2/w_0^2) \times \exp(-ik_{z,m_i} z) [\exp(i\theta) - \exp(-i\theta)] \times \hat{\boldsymbol{\theta}} - i \frac{E_0 x}{z_R} \exp(-r^2/w_0^2) \exp(-ik_{z,m_i} z) \times [\exp(i\theta) + \exp(-i\theta)] \hat{\mathbf{z}}. \quad (46)$$

In a way similar to that in Eqs. (13) and (14), let us calculate

$$E^i_\theta + iE^i_r = iE_0 \exp(-r^2/w_0^2) \exp(-ik_{z,m_i} z) \exp(i\theta), \quad (47)$$

$$E^i_\theta - iE^i_r = -iE_0 \exp(-r^2/w_0^2) \exp(-ik_{z,m_i} z) \exp(-i\theta). \quad (48)$$

We see that only the $(+1)$th and the (-1)th Fourier components appear in Eqs. (47) and (48), respectively. These expressions have to be represented in the discretized form of Eqs. (13) and (14) in order to allow us to find the components b^E_{-1,m_i} and c^E_{1,m_i} in the Fourier–Bessel basis:

$$iE_0 \exp(-r^2/w_0^2) \exp(-ik_{z,m_i} z) = 2c^E_{1,m_i} J_0(k_{m_i} r) \times k_{m_i} \Delta k_{m_i}, \quad (49)$$

$$-iE_0 \exp(-r^2/w_0^2) \exp(-ik_{z,m_i} z) = 2b^E_{-1,m_i} J_0(k_{m_i} r) \times k_{m_i} \Delta k_{m_i}. \quad (50)$$

It is then necessary to multiply the equations by $rJ_0(k_{m_i}, r)$ and to integrate with respect to r from 0 to ∞. Using the properties of Bessel functions [see Eq. (II.4.29) of Ref. 9], one obtains

$$c^E_{1,m_i} = \frac{iE_0}{2\Delta k_{m_i}} \exp(-ik_{z,m_i} z) \frac{w_0^2}{2} \exp(-k^2_{m_i} w_0^2/4) = -b^E_{-1,m_i}, \quad (51)$$

4. DIFFERENTIAL METHOD

A. Presentation of the Method in a Fourier–Bessel Basis

Projecting Maxwell equations onto a Fourier–Bessel basis explicitly allows expression of the derivatives of the electromagnetic field with respect to the variables r and θ. The experience with diffraction gratings shows that it is preferable to formulate the differential method in the form of a set of first-order differential equations with respect to the variable z of the form

$$\frac{d\mathbf{F}_n(z)}{dz} = M_n \mathbf{F}_n(z), \quad n \in [-N, N], \quad (52)$$

where $\mathbf{F}_n$ are column vectors with dimension 4(Max + 1) containing the electromagnetic-field components onto the Fourier–Bessel basis:

$$\mathbf{F}_n = \begin{vmatrix} \tilde{b}^E_{n,m} \\ \tilde{c}^E_{n,m} \\ \tilde{b}^H_{n,m} \\ \tilde{c}^H_{n,m} \end{vmatrix}. \tag{53}$$

The M_n matrices being z independent, the integration of Eq. (52) is made with the use of the eigenvalue/eigenvector technique. The device is invariant with respect to the variable θ so that, as can be seen in Eqs. (5) and (6), the Fourier components are mutually independent. If the structure were modulated with respect to θ, the differential problem would couple the equations for different n in Eq. (52), which would require an M matrix of dimension $4(\mathrm{Max}+1)\times(2N+1)\times 4(\mathrm{Max}+1)\times(2N+1)$. However, when the structure does not present any modulation with respect to θ, one has to integrate $(2N+1)$ Eq. (52) with M_n matrices having dimension $4(\mathrm{Max}+1)\times 4(\mathrm{Max}+1)$.

B. Determination of the Column Vector $\mathbf{F}'_n$

The elements of the M_n matrix are determined from the relation between the components of $\mathbf{F}_n$ and its derivative $\mathbf{F}'_n$ ($\mathbf{F}'_n = \mathrm{d}\mathbf{F}_n/\mathrm{d}z$). The relation between the derivative $\tilde{b}^{E\prime}_{n,m}$ and the components of $\mathbf{F}_n$ are

$$\begin{aligned}\frac{\mathrm{d}}{\mathrm{d}z}(E_{\theta,n} - iE_{r,n}) &= \sum_{m=1}^{\mathrm{Max}} 2k_m\Delta k_m b'^E_{n,m} J_{n+1}(k_m r) \\ &= \frac{in}{r}E_{z,n} - i\omega\mu_0 H_{r,n} - i\frac{\partial E_{z,n}}{\partial r} \\ &\quad + \omega\mu_0 H_{\theta,n}. \end{aligned}\tag{54}$$

Multiplying the two terms by $J_{n+1}(k_{m''}r)r\mathrm{d}r$ and integrating from 0 to infinity, we obtain, with the use of Eq. (28) and the orthogonality property of the Bessel-functions basis, the following relation:

$$\begin{aligned}\tilde{b}'^E_{n,m} &= \omega\mu_0\tilde{b}^H_{n,m} - \frac{k_m}{2\omega}\sum_{m'=1}^{\max}([\tilde{\epsilon}]^{\tilde{n},n}_{\tilde{m},m'})^{-1}k_{m'} \\ &\quad \times [\tilde{b}^H_{n,m'} - \tilde{c}^H_{n,m'}]. \end{aligned}\tag{55}$$

One can calculate in the same way the relation between the derivative $\tilde{b}^{H\prime}_{n,m}$ and the components of $\mathbf{F}_n$:

$$\begin{aligned}\frac{\mathrm{d}}{\mathrm{d}z}(H_{\theta,n} - iH_{r,n}) &= 2\sum_{m=1}^{\infty} k_m\Delta k_m b'^H_{n,m} J_{n+1}(k_m r) \\ &= \frac{1}{r}\frac{\partial H_{z,n}}{\partial\theta} + i\omega\epsilon(r) \\ &\quad \times E_{r,n} - i\frac{\partial H_{z,n}}{\partial r} - \omega\epsilon(r)E_{\theta,n}. \end{aligned}\tag{56}$$

Multiplying the two terms by $J_{n+1}(k_{m''}r)r\mathrm{d}r$ and integrating from 0 to infinity, we obtain

$$\begin{aligned}2\tilde{b}'^H_{n,m} &= \frac{k_m^2}{\omega\mu_0}(\tilde{b}^E_{n,m} - \tilde{c}^E_{n,m}) \\ &\quad + i\omega k_m\int_{r=0}^{\infty}\epsilon(r)E_{r,n}(r)J_{n+1}(k_m r)r\mathrm{d}r \\ &\quad - \omega k_m\int_{r=0}^{\infty}\epsilon(r)E_{\theta,n}(r)J_{n+1}(k_m r)r\mathrm{d}r. \end{aligned}\tag{57}$$

The projection of the product $\epsilon(r)E_{r,n}(r)$ onto the Fourier–Bessel basis has to be made with use of the inverse rule, as extended to the Fourier–Bessel basis in Appendix A:

$$\begin{aligned} ik_m\int_{r=0}^{\infty}\epsilon(r)E_{r,n}(r)J_{n+1}(k_m r)r\mathrm{d}r &= -\sum_{m'=1}^{\mathrm{Max}}\sum_{m''=1}^{\mathrm{Max}}([\Psi]^{\widetilde{n-1,n+1}})_{m,m''}\left(\left[\frac{1}{\epsilon}\right]^{\widetilde{n+1,n+1}}\right)^{-1}_{m'',m'} \\ &\quad \times \tilde{b}^E_{n,m'} + \sum_{m'=1}^{\mathrm{Max}}\left(\left[\frac{1}{\epsilon}\right]^{\widetilde{n-1,n-1}}\right)^{-1}_{m,m'}\tilde{c}^E_{n,m'}, \end{aligned}\tag{58}$$

where

$$[\Psi]^{\widetilde{n-1,n+1}}_{m,m''} = k_m\Delta k_m\int_{r=0}^{\infty}J_{n-1}(k_m r)J_{n+1}(k_{m''}r)r\mathrm{d}r. \tag{59}$$

All the terms of the matrix $[\Psi]^{\widetilde{n-1,n+1}}$ have analytical expressions given in Ref. 9. The projection of the product $\epsilon(r)E_{\theta,n}$ onto the Fourier–Bessel basis is done by using the direct rule (Appendix A):

$$\begin{aligned}\int_{r=0}^{\infty}k_m\epsilon(r)E_{\theta,n}J_{n+1}(k_m r)r\mathrm{d}r &= \sum_{m'=1}^{\mathrm{Max}}[\epsilon]^{\widetilde{n+1,n+1}}_{m,m'}\tilde{b}^E_{n,m'} + \sum_{m'=1}^{\max}[\epsilon]^{\widetilde{n+1,n-1}}_{m,m'}\tilde{c}^E_{n,m'}. \end{aligned}\tag{60}$$

The components $\tilde{c}'^E_{n,m}$ and $\tilde{c}'^H_{n,m}$ are calculated in the same way, using a sum instead of subtracting in the first term of Eqs. (54) and (56), and replacing the Bessel function $J_{n+1}(k_m r)$ in the scalar products by the Bessel function $J_{n-1}(k_m r)$.

C. Expression of the M_n-Matrix Elements

Using the results obtained in Subsection 4.B, we are able to write the expressions of the elements of the M_n matrix. We introduce submatrices $M_{n,ij}$ with dimension $2(\mathrm{Max}+1)\times 2(\mathrm{Max}+1)$:

$$M_n = \begin{bmatrix} M_{n,11} & M_{n,12} \\ M_{n,21} & M_{n,22} \end{bmatrix}, \tag{61}$$

where matrices $M_{n,ij}$ are determined according to the Subsection 4.B:

where $K_{mn} = k_m\delta_{mn}$, $\mathrm{I}_{mn} = \delta_{mn}$, $m,\ n \in [1, \mathrm{Max}]$. Since $M_{n,11} = 0$ and $M_{n,22} = 0$, the derivatives $\tilde{b}'^E_{n,m}$ and $\tilde{c}'^E_{n,m}$ (resp. $\tilde{b}'^H_{n,m}$ and $\tilde{c}'^H_{n,m}$) depend only on the components $\tilde{b}^H_{n,m}$ and $\tilde{c}^H_{n,m}$ (resp. $\tilde{b}^E_{n,m}$ and $\tilde{c}^E_{n,m}$).

$$M_{n,11} = 0,$$

$$M_{n,12} = \begin{bmatrix} -\frac{1}{2\omega}K[\epsilon^{\tilde{n},n}]^{-1}K + \omega\mu_0 \mathrm{I} & -\frac{1}{2\omega}K[\epsilon^{\tilde{n},n}]^{-1}K \\ -\frac{1}{2\omega}K[\epsilon^{\tilde{n},n}]^{-1}K & \frac{1}{2\omega}K[\epsilon^{\tilde{n},n}]^{-1}K - \omega\mu_0 I \end{bmatrix},$$

$$M_{n,21} = \begin{bmatrix} \frac{K^2}{2\omega\mu_0}\mathrm{I} - \frac{\omega}{2}\left(\left[\frac{1}{\epsilon}^{\widetilde{n+1,n+1}}\right]^{-1} + [\epsilon^{\widetilde{n+1,n+1}}]\right) & -\frac{K^2}{2\omega\mu_0}\mathrm{I} + \frac{\omega}{2}\left([\Psi]^{\widetilde{n+1,n-1}}\left[\frac{1}{\epsilon}^{\widetilde{n-1,n-1}}\right]^{-1} - [\epsilon^{\widetilde{n+1,n-1}}]\right) \\ \frac{K^2}{2\omega\mu_0}\mathrm{I} - \frac{\omega}{2}\left([\Psi]^{\widetilde{n-1,n+1}}\left[\frac{1}{\epsilon}^{\widetilde{n+1,n+1}}\right]^{-1} - [\epsilon^{\widetilde{n-1,n+1}}]\right) & -\frac{K^2}{2\omega\mu_0}\mathrm{I} + \frac{\omega}{2}\left(\left[\frac{1}{\epsilon}^{\widetilde{n-1,n-1}}\right]^{-1} + [\epsilon^{\widetilde{n-1,n-1}}]\right) \end{bmatrix},$$

$$M_{n,22} = 0, \tag{62}$$

The present method of writing Maxwell equations in a truncated basis, called fast Fourier factorization method in the diffraction-grating theory,[2,3] is called fast numerical factorization (FNF) method when one is dealing with arbitrary truncated basis of continuous functions. When the correct rules are not used, the inverse rule is replaced by the direct one, and the following substitutions have to be made:

$$\left[\frac{1}{\epsilon}^{\widetilde{n+1,n+1}}\right]^{-1} \rightarrow [\epsilon^{\widetilde{n+1,n+1}}], \quad \left[\frac{1}{\epsilon}^{\widetilde{n-1,n-1}}\right]^{-1} \rightarrow [\epsilon^{\widetilde{n-1,n-1}}]. \tag{63}$$

5. NUMERICAL IMPLEMENTATION

A. Near-Field Map Calculations in the Vicinity of a Glass Cylinder

To demonstrate the possibilities of the method, we first consider the diffraction of light by a cylinder made of glass, lying below the surface of a plane dielectric of the same dielectric permittivity. The exit substrate is air. We illuminate the device from the superstrate in normal incidence by a plane wave with wavelength of 647 nm. The electric field is polarized parallel to the Oy axis [perpendicular to the Oxz plane represented in Figs. 2(a) and 2(b)]. The height of the cylinder is 100 nm, and its diameter is taken equal to the wavelength. Figures 2(a) and 2(c) present the near-field map in the Oxz and Oxy plane, and Fig. 2(b) shows the Poynting vector. The convergence of the method has been studied and is quite fast. Reducing the integration step Δk_r or increasing the ratio $k_{r,\mathrm{Max}}/k_0$ compared with the ones chosen for the calculations (given in the figure caption) does not bring any change in the results.

In Fig. 2(a), one can observe a focalization of the light in an area around a point of the z axis with coordinate $z = -400\,\mathrm{nm}$. A confirmation is given in Fig. 2(b), showing the direction and values of the Poynting vector. The darker the arrow, the stronger the Poynting vector modulus. The Poynting vector deviates from the z axis above the cylinder ($z = 125\,\mathrm{nm}$) and converges below the cylinder toward the z axis. It looks as if the glass cylinder were working like a lens with a short focal distance. However, no simple physical explanation can be given for this phenomenon, which appears far outside the Gaussian approximation of optics.

Finally, Fig. 2(c) represents the field map in the Oxy plane below the cylinder. As can be observed, although the structure is θ independent, the polarization of the incident plane wave leads to variations of the electric field with respect to θ.

B. Cylindrical Hole in a Plane Metallic Screen

The method is suitable for modeling diffraction by a single or structured hole pierced in a metallic screen. To study its possibilities, we have chosen two examples of circular holes having different radius pierced in a silver screen with 200-nm thickness having a relative permittivity $\epsilon_{\mathrm{Ag}} = -8 + i3$ at 500-nm wavelength.

In the first example, the hole diameter is equal to the wavelength ($R = 250\,\mathrm{nm}$). Figure 3 presents the values of $|E_r|$ calculated on the z axis at a point situated 15 nm below the screen, as a function of the truncation parameter $k_{r,\mathrm{Max}}$ for two different values of the integration constant $\Delta k_r = 0.0003\,\mathrm{nm}^{-1}$ and $0.0006\ \mathrm{nm}^{-1}$. No visible difference is observed between the results obtained with these values of Δk_r. On the contrary, the results depend significantly on the truncation parameter and on the method used. When applying the correct factorization rules (FNF), the convergence with respect to $k_{r,\mathrm{Max}}/k_0$ is much faster than the method without FNF [Eq. (63)]. This difference is even more pronounced in the spatial near-field distribution. Figure 4 shows the r dependence of $|E_r|$ 15 nm below the slab for different values of Max (i.e., of $k_{r,\mathrm{Max}}/k_0$). As observed in Fig. 4(b), with the FNF method, Max = 400 (corresponding to $k_{r,\mathrm{Max}}/k_0 = 9.6$) is already sufficient to obtain satisfactory results, presenting no difference from Max = 800. When comparing Figs. 4(b) and 4(c), one can see clearly that without FNF [Eq. (63)] the results contain Gibbs' phenomenon owing to the discontinuity of $|E_r|$ across the hole boundaries, a phenomenon that is absent when the FNF rules are used. Figure 5 shows the spatial distribution of $|E_z|$, presenting sharp peaks at the hole boundaries. In the second example, presented in Figs. 6 and 7, the hole radius is ten times smaller ($R = 25\,\mathrm{nm}$). Figure 6 pre-

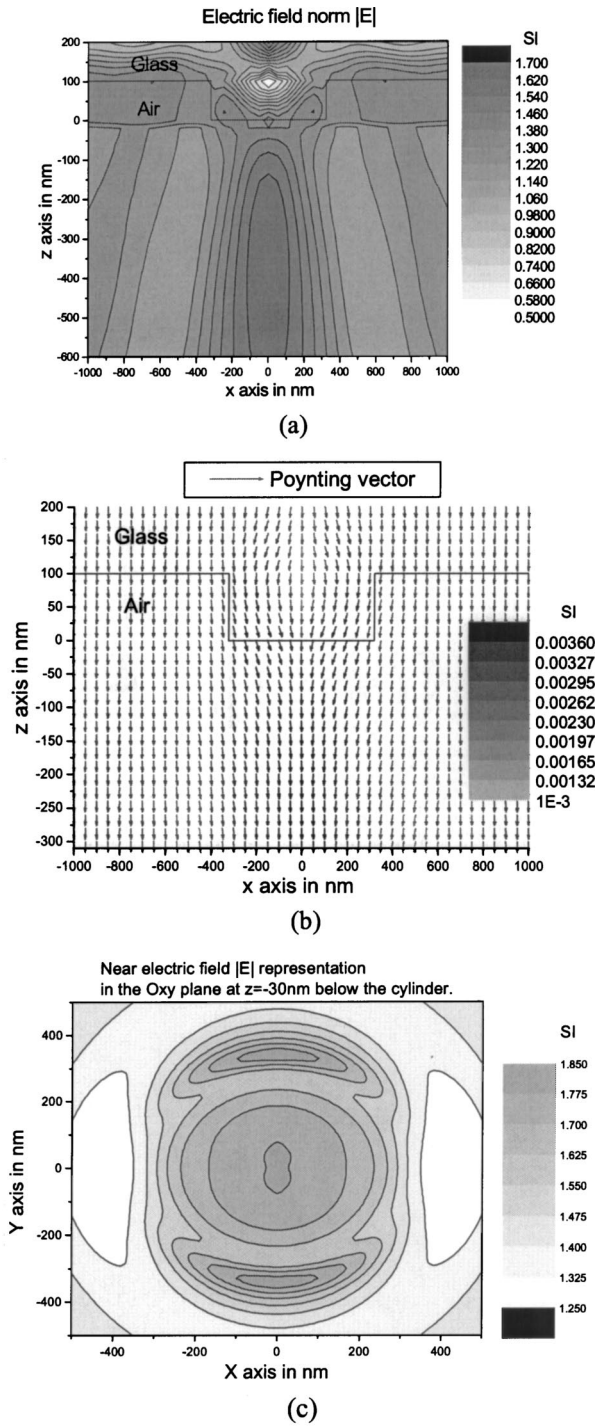

Fig. 2. Representations of the near field. The superstrate is glass with a relative dielectric permittivity $\epsilon_r = 2.28$. The substrate is air. The device is illuminated in normal incidence with wavelength of 647 nm. The thickness of the cylinder is 100 nm, and its diameter is taken equal to the wavelength. (a) Near-electric-field map in the Oxz plane, (b) Poynting vector, (c) shows electric-field $|\mathbf{E}|$ map in the Oxy plane. $\Delta k_r = 0.001\,\mathrm{nm}^{-1}$, $k_{r,\mathrm{Max}}/k_0 = 6.001$, $N = 4$.

sents the convergence of the value of $|E_r|$ as a function of the truncation parameter in the same way as was done in Fig. 3 for $R = 250\,\mathrm{nm}$. Without the FNF approach, no convergence is observed. Owing to the small hole dimension, it is necessary to go much farther into the k space, so that now even with use of the correct FNF rules [Figs. 7(a) and 7(b)], the value of $k_{r,\mathrm{Max}}/k_0 = 9.6$ corresponding to Max = 400 is not sufficient to present the spatial field distribution correctly [compare Figs. 7(a) and 7(b), in contrast to the previous case [Fig. 4(b)] when the hole was much wider. Without FNF, the fine structure of the field is not well represented even for values of $k_{r,\mathrm{Max}}/k_0$ approaching 20 [Fig. 7(c)].

Finally, during the testing of the code, we observed some difficulties for highly conducting metals. This is not surprising, as the differential method (as well as the rigorous coupled-wave approach, in particular) also presents some difficulties with high conductivity.[10] The convergence with respect to $k_{r,\mathrm{Max}}$ becomes slower when, for example, it is necessary to model aluminum, having larger relative permittivity in the visible, $\epsilon_{\mathrm{Al}} = -50 + i20$. Moreover, owing to the smaller absorption losses, the plasmon anomaly in the highly conducting metals becomes sharper and requires smaller values of the integration step Δk_r. The combination of these two requirements makes the computation difficult, because it needs much larger matrices than in the cases presented in Figs. 3–7. And it is necessary to point out that even in the latter cases the matrices are already very large. For example, Max = 800 requires solution of 3200 equations with 3200 unknowns.

A similar difficulty is observed when one is studying diffraction by objects much larger than the wavelength, because these objects require a much smaller integration step (the field variations in the k space become more rapid).

Although it is not the aim of this paper, which is devoted to theory, to present an extensive study of the extraordinary transmission through subwavelength holes, it is interesting to study the spectral variation of the electric-field pattern and to compare the numerical results with those obtained in a recent experiment.[11] To that end, using the same device as preceding, we study the near field at $z = -40\,\mathrm{nm}$ below the hole with a radius R equal to 135 nm. Although the code is able to take into

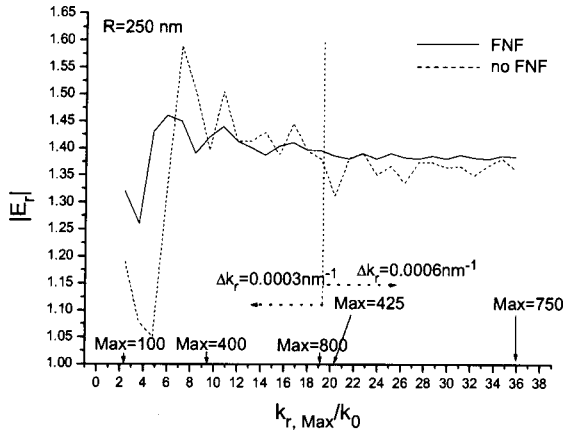

Fig. 3. Convergence of the near-field amplitude as a function of the truncation parameter $k_{r,\mathrm{Max}}$, normalized with respect to the incident wave number k_0. The results represent the value of $|E_r|$ at a point on the z axis situated 15 nm below the hole opening. Solid curve, FNF method; dashed curve, without FNF. The working parameters (Δk_r and m) are represented in the figure. $R = 250\,\mathrm{nm}$.

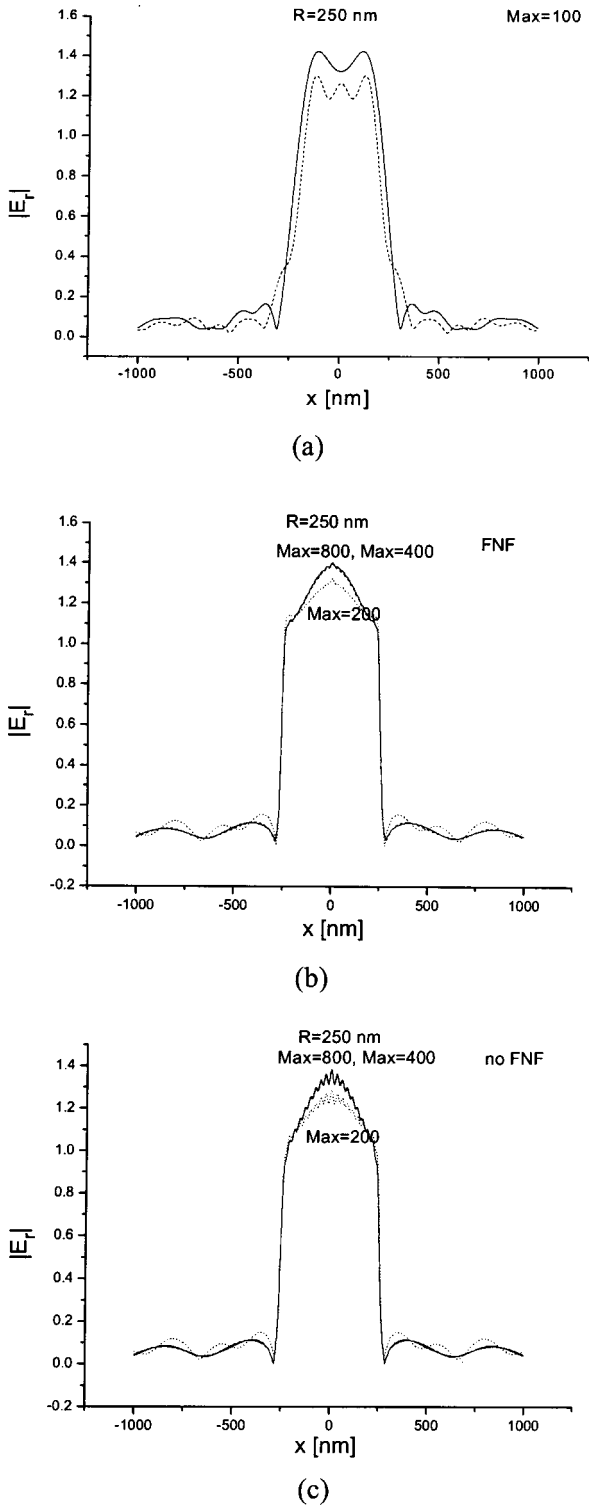

Fig. 4. Near-field distribution of $|E_r|$ ($\theta = 0$) in the x direction for different working parameters, calculated 15 nm below the hole opening. $\Delta k_r = 0.0003\,\mathrm{nm}^{-1}$. (a) Max = 100, $k_{r,\max}/k_0 = 2.387$. Solid curve, FNF; dashed curve, without FNF. (b) dotted curve, Max = 200; dashed curve, Max = 400; solid curve, Max = 800. FNF method. (c) Same as (b) but without FNF.

account the dispersion of the permittivity, for better visibility of the results we do not use it in the study. We then plot the maximum of $|E|^2$ when x and y are varied in the plane $z = -40\,\mathrm{nm}$ as a function of wavelength. Figure 8 shows the spectral dependence of $|E|^2$. One observes a well-expected gradual decline of transmission when increasing the wavelength from 200 to 400 nm. However, an unexpected second maximum at $\lambda \approx 750\,\mathrm{nm}$ is observed. This confirms recent experimental observations.[11] In Fig. 1 of Ref. 11, the authors analyzed the transmittance of a single hole of 270-nm diameter pierced in Ag films with different thicknesses. In particular, when thickness was equal to 200 nm, the transmittance presented a spectral dependence similar to the one shown in Fig. 8. The phenomenological explanation of that behavior requires further study.

6. CONCLUSION

We have presented a new formulation of the differential method in cylindrical coordinates, suitable for modeling diffraction by systems having finite axial dimensions. At present, the theory seems particularly well adapted to study of the near-electric-field map inside and outside devices such as holes, modulated or not, pierced in a metallic plane and dielectric or metallic cylinders with finite dimensions. The method is rapidly converging in the case of dielectric devices and still has a fast enough convergence when one is dealing with silver objects.

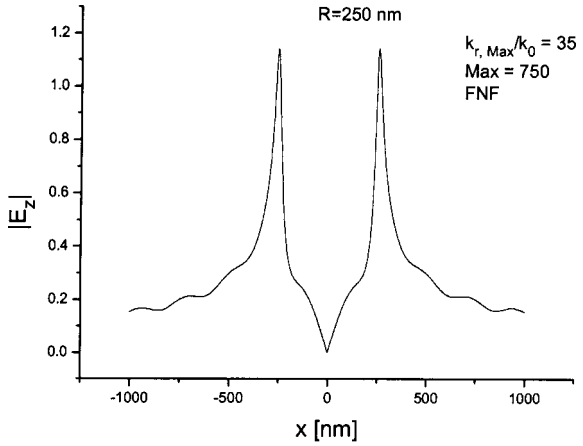

Fig. 5. Radial distribution of $|E_z|$ 15 nm below the hole opening (FNF method).

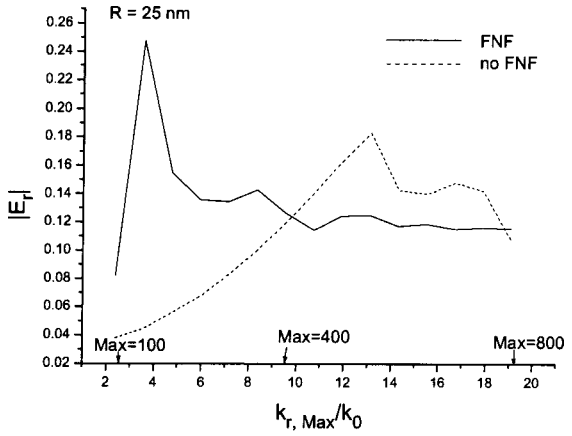

Fig. 6. Same as Fig. 3 but for $R = 25\,\mathrm{nm}$. $\Delta k_r = 0.0003\,\mathrm{nm}^{-1}$.

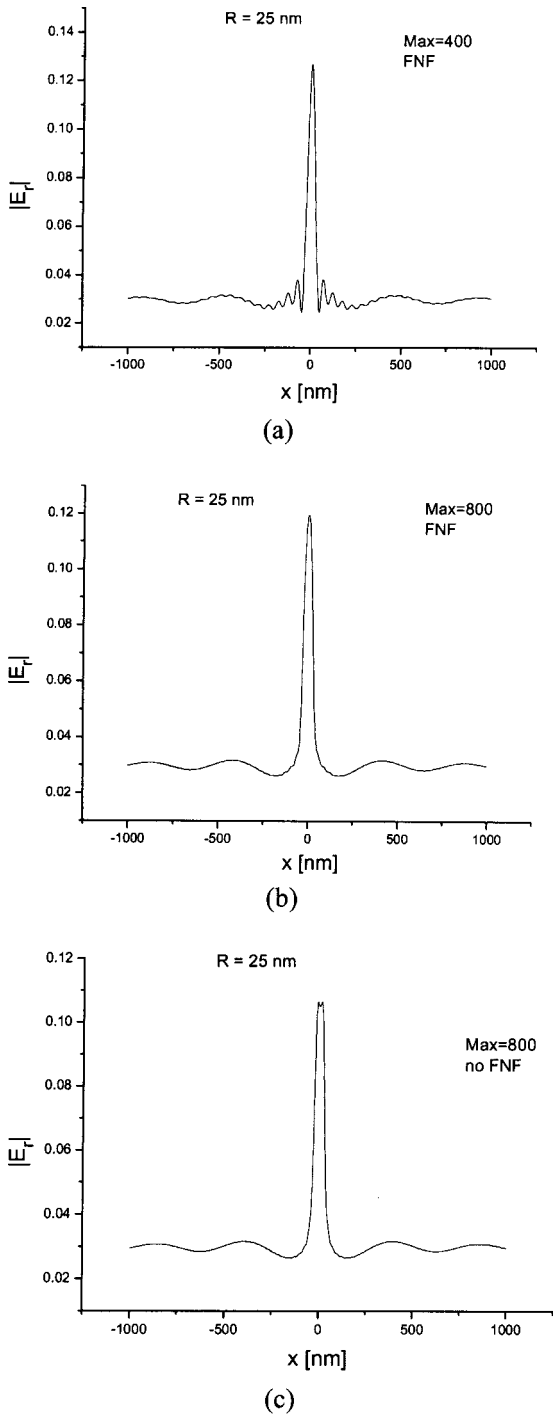

Fig. 7. $|E_r|$ as a function of x for $\theta = 0$ calculated with $\Delta k_r = 0.0003\,\mathrm{nm}^{-1}$ 15 nm below the hole with $R = 25\,\mathrm{nm}$. (a) Max = 400 (FNF), (b) Max = 800 (FNF), (c) Max = 800 without FNF.

APPENDIX A: FACTORIZATION RULES

1. Direct Rule $[D_{\theta,n}(r)=\epsilon(r)E_{\theta,n}(r)]$

We present the calculation of the scalar product of the product of functions $\epsilon(r)E_{\theta,n}(r)$ with the Bessel function $J_{n+1}(k_m r)$:

$$\int_{r=0}^{\infty} k_m \epsilon(r) E_{\theta,n} J_{n+1}(k_m r) r\,\mathrm{d}r. \tag{A1}$$

The function $E_{\theta,n}(r)$ is continuous. Thus it can be represented by the truncated series of Bessel functions shown in Eq. (18). Putting this sum into Eq. (A1), we obtain

$$\begin{aligned}\sum_{m'=1}^{\mathrm{Max}} \tilde{b}^{E}_{n,m'} k_m \Delta k_{m'} \int_{r=0}^{\infty} \epsilon(r) J_{n+1}(k_{m'} r) J_{n+1}(k_m r) r\,\mathrm{d}r \\ + \sum_{m'=1}^{\mathrm{Max}} \tilde{c}^{E}_{n,m'} k_m \Delta k_{m'} \\ \times \int_{r=0}^{\infty} \epsilon(r) J_{n-1}(k_{m'} r) J_{n+1}(k_m r) r\,\mathrm{d}r \\ = \sum_{m'=1}^{\mathrm{Max}} \tilde{b}^{E}_{n,m'} k_m \Delta k_m [\epsilon]^{n+1,n+1}_{m,m'} \\ + \sum_{m'=1}^{\mathrm{Max}} \tilde{c}^{E}_{n,m'} k_m \Delta k_m [\epsilon]^{n+1,n-1}_{m,m'}. \end{aligned} \tag{A2}$$

2. Inverse Rule $[D_{r,n}(r)=\epsilon(r)E_{r,n}(r)]$

We present the calculation of the scalar product of the product of functions $\epsilon(r)E_{r,n}(r)$ with the Bessel function $J_{n-1}(k_m r)$:

$$\int_{r=0}^{\infty} k_m \epsilon(r) E_{r,n} J_{n-1}(k_m r) r\,\mathrm{d}r = D_{r,n,m}. \tag{A3}$$

The function $E_{r,n}(r)$ is discontinuous; thus we cannot represent it as a truncated series of Bessel functions, because of the poor convergence that would occur. We have to develop the continuous product of functions $D_{r,n} = \epsilon(r)E_{r,n}(r)$:

$$D_{r,n} = \sum_{m=1}^{\mathrm{Max}} D_{r,n,m} J_{n-1}(k_m r) k_m \Delta k_m. \tag{A4}$$

We must calculate the components $D_{r,n,m}$ as functions of the components $E_{r,n,m}$. We then write

$$E_{r,n} = \sum_{m=1}^{\mathrm{Max}} \frac{1}{\epsilon(r)} D_{r,n,m} J_{n-1}(k_m r) k_m \Delta k_m. \tag{A5}$$

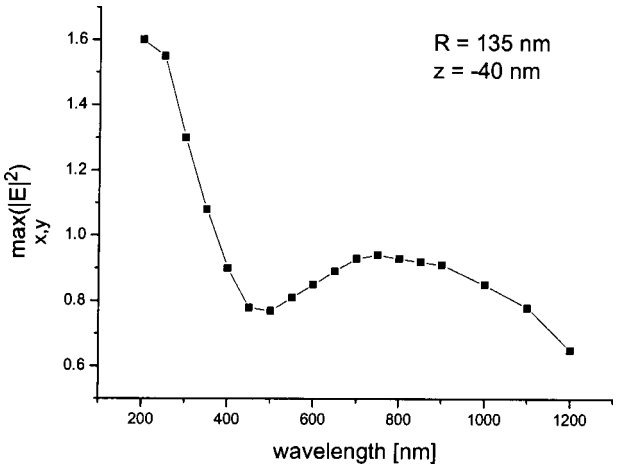

Fig. 8. Spectral dependence of the maximum of $|E|^2$ in the plane $z = -40\,\mathrm{nm}$, $R = 135\,\mathrm{nm}$. The dispersion of the permittivity is not taken into account.

Its scalar product with the function $J_{n-1}(k_m r)$ reads as

$$E_{r,n,m'} = \int_{r=0}^{\infty} E_{r,n} J_{n-1}(k_{m'} r) r \mathrm{d}r = \sum_{m=1}^{\mathrm{Max}} D_{r,n,m} k_m \Delta k_m \int_{r=0}^{\infty} \frac{1}{\epsilon(r)} \times J_{n-1}(k_m r) J_{n-1}(k_{m'} r) r dr, \quad \text{(A6)}$$

$$k_{m'} E_{r,n,m'} = \sum_{m=1}^{\mathrm{Max}} \left[\frac{1}{\epsilon}\right]^{\widetilde{n-1,n-1}}_{m',m} k_m D_{r,n,m}. \quad \text{(A7)}$$

By inverting the matrix $[1/\epsilon]^{\widetilde{n-1,n-1}}$, we obtain the expression of $D_{r,n,m}$:

$$k_m D_{r,n,m} = \sum_{m'=1}^{\mathrm{Max}} \left(\left[\frac{1}{\epsilon}\right]^{\widetilde{n-1,n-1}}\right)^{-1}_{m,m'} k_{m'} E_{r,n,m'}. \quad \text{(A8)}$$

At this stage, we have to calculate the term $E_{r,n,m'}$, which is a scalar product of the function $E_{r,n}$ with the Bessel function $J_{n-1}(k_m r)$. With Eqs. (17) and (59), this scalar product reads as

$$ik_{m'} E_{r,n,m'} = k_{m'} \sum_{m''=1}^{\mathrm{Max}} (-\tilde{b}^E_{n,m''} \Delta k_{m''} [\Psi]^{\widetilde{n+1,n-1}}_{m'',m'}) + \tilde{c}^E_{n,m'}. \quad \text{(A9)}$$

Replacing $E_{r,n,m'}$ in Eq. (A8), one obtains

$$ik_m D_{r,n,m} = -\sum_{m'=1}^{\mathrm{Max}} \sum_{m''=0}^{\mathrm{Max}} \left(\left[\frac{1}{\epsilon}\right]^{\widetilde{n-1,n-1}}\right)^{-1}_{m,m''} \times ([\Psi]^{\widetilde{n-1,n+1}})_{m'',m} \tilde{b}^E_{n,m'} + \sum_{m'=1}^{\mathrm{Max}} \left(\left[\frac{1}{\epsilon}\right]^{\widetilde{n-1,n-1}}\right)^{-1}_{m,m'} \tilde{c}^E_{n,m'}, \quad \text{(A10)}$$

$$ik_m D_{r,n,m} = -\sum_{m'=1}^{\mathrm{Max}} \sum_{m''=0}^{\mathrm{Max}} ([\Psi]^{\widetilde{n-1,n+1}})_{m,m''} \times \left(\left[\frac{1}{\epsilon}\right]^{\widetilde{n+1,n+1}}\right)^{-1}_{m'',m'} \tilde{b}^E_{n,m'} + \sum_{m'=1}^{\mathrm{Max}} \left(\left[\frac{1}{\epsilon}\right]^{\widetilde{n-1,n-1}}\right)^{-1}_{m,m'} \tilde{c}^E_{n,m'}. \quad \text{(A11)}$$

REFERENCES

1. P. Vincent, "Differential methods," in *Electromagnetic Theory of Gratings*, R. Petit, ed. (Springer-Verlag, Berlin, 1980), Chap. 4.
2. M. Nevière and E. Popov, *Light Propagation in Periodic Medias: Differential Theory and Design* (Marcel Dekker, New York, 2003).
3. E. Popov and M. Nevière, "Maxwell equations in Fourier space: fast converging formulation for diffraction by arbitrary shaped, periodic, anisotropic media," J. Opt. Soc. Am. A **18**, 2886–2894 (2001).
4. B. Guizal, D. Barchiesi, and D. Felbacq, "Electromagnetic beam diffraction by a finite lamellar structure: an aperiodic coupled-wave method," J. Opt. Soc. Am. A **20**, 2274–2280 (2001).
5. J. D. Jackson, *Classical Electromagnetism*, 3rd ed. (Wiley, New York, 1998), Chap. 3.
6. L. Li, "Use of Fourier series in the analysis of discontinuous periodic structures," J. Opt. Soc. Am. A **13**, 1870–1876 (1996).
7. E. Popov, M. Nevière, and N. Bonod, "Factorization of products of discontinuous functions applied to Fourier–Bessel basis," J. Opt. Soc. Am. A **21**, 46–52 (2004).
8. L. W. Davis, "Theory of electromagnetism beams," Phys. Rev. A **19**, 1177–1179 (1979).
9. M. Abramovitz and I. A. Stegun, eds., *Handbook of Mathematical Functions* [9th printing (1970).] National Bureau of Standards Applied Mathematics Series 55 (U.S. Government Printing Office, Washington, D.C., 1964).
10. E. Popov, B. Chernov, M. Nevière, and N. Bonod, "Differential theory: application to highly conducting gratings," J. Opt. Soc. Am. A **21**, 199–206 (2004).
11. A. Degiron, H. J. Lezec, N. Yamamoto, and T. W. Ebbesen, "Optical transmission properties of a single subwavelength aperture in a real metal," Opt. Commun. **239**, 61–66 (2004).